Applied Physics A (2022) 128: 819
https://doi.org/10.1007/s00339-022-05965-4

Applied Physics A
Materials Science & Processing

Enhanced linear and nonlinear optical properties of erbium/ytterbium lead phosphate glass by gamma irradiation for optoelectronics applications

O. I. Sallam[1] · M. I. A. Abdel Maksoud[2] · Said M. Kassem[3] · A. S. Awed[4] · N. A. Elalaily[1]

Received: 12 May 2022 / Accepted: 13 August 2022 / Published online: 24 August 2022

Abstract
Herein, this study intends to reveal the impact of gamma irradiation on the structural, linear, and nonlinear optical characteristics of $47P_2O_5-23Na_2O-6Al_2O_3-22PbO-0.5Er_2O_3-1.5Yb_2O_3$ glass. The Er/Yb-doped lead phosphate glass samples were produced using the traditional melt quenching procedure and then treated to different doses of gamma irradiation (0, 20, 50, and 100) kGy. The amorphous phase structure of the Er/Yb-doped lead phosphate glass samples was verified through XRD patterns. Also, the shift of the FTIR peaks due to the change in bond angles, and the change in the bond length of the P–O–P bridges means the glass network stability against radiation. With increasing irradiation dosages, the energy gap dropped from 4.11 eV to 3.42 eV and then enhanced to 3.48 at 100 kGy. At the same time, the Urbach energy enhanced from 10.23 eV to 37.03 eV. The oscillator energy Eo was found between 1.55 and 1.62 eV. Also, the dispersion energy E_d varied between 2.11 eV at 100 kGy and 2.71 eV at the dose of 50 kGy. The percentage of free carrier ions to effective mass (N/m*) is in the range $(4.82–8.66)\times10^{47}$ cm^3/g. Besides, the lattice dielectric constant (ε_l) increased from 5.54 to 6.63 as the gamma dosages increased. Furthermore, increasing gamma doses up to 50 kGy promotes susceptibility, which subsequently declines at 100 kGy, suggesting that increasing gamma doses over 50 kGy weakens polarizability potential. While the increasing gamma doses up to 50 kGy reduces the nonlinear refractive index and then improves at 100 kGy. Overall, the nonlinear and linear research revealed that Er/Yb lead phosphate glass is being used as a promising material for gain media and optical amplifiers.

Keywords Erbium/ytterbium lead phosphate glasses · Linear optical properties · Dielectric constants · Gamma irradiation

1 Introduction

The scientific community has recently focused on manufacturing and analyzing optical glass systems doped with heavy metal oxide (HMO) and its special applications in optics, photonic devices, and nuclear engineering [1–5]. Synthesis and characterization of new materials are important for several applications [6–11]. Furthermore, doping such substances with rare-earth (Re^{3+}) ions enhances their optical and electronic properties, good stability, and flexibility characteristics, allowing an intake of elements in their formulation to be accepted. While also lasers, solid-phase lighting systems, fiber amplification, photodetectors, storage systems, dosimeters, and renewable power their uses are advancing [2, 12–17]. Moreover, trivalent rare-earth (Re^{3+}) ions in glasses contain a substantial percentage of absorption bands in the Vis–NIR areas, making them useful as practical photonic elements for various purposes. Specifically, Er^{3+}/

✉ M. I. A. Abdel Maksoud
muhamadmqsod@gmail.com;
muhamad.abdelmaksoud@eaea.org.eg

1 Glass lab., Radiation Chemistry Department, National Center for Radiation Research and Technology (NCRRT), Egyptian Atomic Energy Authority (EAEA), Cairo, Egypt

2 Radiation Physics Department, National Center for Radiation Research and Technology (NCRRT), Egyptian Atomic Energy Authority (EAEA), Cairo, Egypt

3 Radiation Protection and Dosimetry Department, National Center for Radiation Research and Technology (NCRRT), Egyptian Atomic Energy Authority (EAEA), Cairo, Egypt

4 Higher Institute for Engineering and Technology at Manzala, Manzala, Egypt

Yb^{+3} ions activated glasses are valuable as the optical gain host, focusing on producing photonic technologies, including solid-state illumination, color displays, and broad bandwidth data storage capacities [1, 13, 18–21].

Phosphate glass doped with Re^{3+} ions is far from many other materials in terms of realizing photonic materials with enhanced optical gain across a short length while minimizing nonlinear optical consequences, thus leading to high-laser reliability and long-term stability [3, 22, 23]. Lead phosphate glasses with Re^{3+} ions are part of an enormous family of heavy metal glasses explored for potential optoelectronic characteristics as prospective laser glass hosts [24]. Glasses composed of lead-based phosphates are desirable in optoelectronics and therapeutic uses [19, 25].

Co-doping Er^{3+}/Yb^{3+} has been demonstrated to be an effective strategy for producing short, efficient lasers and amplifying the entire communications wavelength region. Doping using Yb^{3+} enhances absorption pumping near ~ 980 nm and energy transfer efficiency between Er^{3+} and Yb^{3+}, allowing for centimeter-long laser beams at low Er^{3+} contents [26]. These glasses' optical, electrical, chemical, and fluorescence characteristics are predominantly improved by adding certain oxides, such as Al_2O_3, PbO, and Na_2O, with rare-earth ions [27–32].

Lead oxide can operate as a glass former or a modifier based on the link between lead and oxide (covalent or ionic), and the PbO/P_2O_5 ratio in the glass network was found to be beneficial for spectroscopy approaches. The chemical resistance of the glass system is improved by the P–O–Pb bond and the lead phosphate's regional geometry. Increasing the number of NBO (non-bridging oxygen) atoms in the host by adding three metal oxide elements can improve its chemical resistance. Furthermore, the presence of lead ions (Pb^{2+}) will significantly benefit the spectroscopic characterization of Re^{3+} ions. Due to the S–P electronic transition of Pb^{2+} ions, there is also a high absorption in the UV area [12, 19, 33, 34].

When aluminum ions are integrated into glass hosts, the fluorescence of rare-earth ions, such as Re^{3+}, is often enhanced because the Al^{3+} ions separate the rare-earth ions from the RE−O−RE bonds and produce Al–O–RE bonds. In contrast to the alumina-free glass hosts, this declustering action results in higher spacing between RE ions, which improves fluorescence emission [19]. In addition, because of its various qualities such as high solubility, enhanced chemical stability, and thermo-mechanical strength. Na_2O is frequently used to adjust low field intensity cations, with Na^+ improving the mechanical qualities necessary for effective laser glass [12, 27, 35].

Researchers studied the effects of gamma irradiation on HMO-based glasses based on the mechanisms of interactions that can be categorized as photoelectric effects, Compton scattering, or pair production [36, 37]. Gamma irradiation causes either the introduction of new active defects or the activation of existing defects and the repair of these defects by recombination or recovery. Irradiation causes changes in the glass matrix's structure, including defects [30, 38]. Optical spectra (UV–Vis light) are used to investigate the impact of radiation on glasses modified with rare-earth oxides that produce distinct emission bands in the UV–visible region [39]. Liberated electrons can pass through the glass matrix during the irradiation process, generating electron–hole pairs that are predicted to interact with non-bridging oxygen that occurs as defects in the host glass to capture the positive holes or liberated radicals, causing color centers to form in the glass network [27].

Ramesh et al. showed that the nonlinear optical (NLO) features improved with gamma irradiation doses increasing, suggesting that high-dose irradiated glasses might be valuable for photonic devices, especially optical limiters. It is worth noting that this study shows how gamma irradiation affects the NLO characteristics of lead phosphate glasses having Re^{3+} ions (Er^{3+}/Yb^{3+} doped and co-doped). Research on the performance of radiation on Re^{3+} doped and co-doped glasses is increasing attention in the photonics and dosimetry investigation fields [1, 40, 41].

Herein, this study intends to reveal the impacts of gamma irradiation on the structural, linear, and nonlinear optical characteristics of $47P_2O_5-23Na_2O-6Al_2O_3-22PbO-0.5Er_2O_3-1.5Yb_2O_3$ glass. The Er/Yb-doped lead phosphate glass sample was produced using the traditional melt quenching procedure and then treated to different doses of gamma irradiation (0, 20, 50, and 100) kGy. Also, our study guides the commercial preparation of Er^{3+}/Yb^{3+} co-doped lead phosphate glasses and active optoelectronic devices.

2 Materials and methods

2.1 Er^{3+}/Yb^{3+}doped lead phosphate glasses preparation

Glass sample with the composition of $47P_2O_5-23Na_2O-6Al_2O_3-22PbO-0.5Er_2O_3-1.5Yb_2O_3$ was prepared by the quenching melting method at 1100 °C at a muffle furnace during the melting process, the molten sample was stirred two times to obtain homogeneity for the molten components of the glassy sample. The molten glassy sample was poured into preheated stainless steel frames, followed by transferring the poured sample into another furnace at 300 °C to avoid thermal stress and let to cool gradually till it reached room temperature after 24 h. The obtained sample was divided into rectangle pieces and power for different measurements [42, 43]. According to the chemical composition formula, the sample has density of 4.15 g/

cm^3. The raw materials used for preparation are ammonium dihydrogen phosphate, sodium carbonate, aluminum oxide, lead oxide, erbium oxide, and ytterbium oxide.

2.2 Characterization of Er/Yb-doped lead phosphate glass samples

The structures of the Er^{3+}/Yb^{3+} co-doped lead phosphate glasses were examined using X-ray diffraction (XRD; Shimadzu XRD-6000, Japan) [44–53]. FTIR absorption spectra of the Er^{3+}/Yb^{3+} co-doped lead phosphate glasses samples were measured via (Thermo Nicolet 380 spectrometer). In addition, the linear and nonlinear optical characteristics were determined using (Jasco, V-570) [42, 43, 45, 54, 55].

3 Results and discussions

3.1 X-ray diffraction (XRD) studies

Figure 1 demonstrates the XRD patterns of Er/Yb-doped lead phosphate glass samples. Besides a broadening hump, XRD patterns revealed no crystalline peaks, suggesting that the Er/Yb-doped lead phosphate glass samples are noticeably amorphous. The Er/Yb-doped lead phosphate glass samples showed no crystalline peaks after being irradiated with gamma radiation. As a result of the wide hump and the absence of crystalline peaks, the Er/Yb-doped lead phosphate samples have an amorphous characteristic both before and after gamma irradiation [42, 43, 56].

4 Fourier transform infra-red (FTIR) studies

Phosphorus pentoxide has a molecular formula, $P_4O_{10,}$ but its common name is derived from the empirical formula (P_2O_5). Phosphate glass is inorganic polymeric [57]. Phosphate glasses have a tetrahedral structure surrounded by four oxygen atoms, and each pair can only share one oxygen ion with the other [58, 59]. In the phosphorus tetrahedral structure, three oxygen atoms bridge to neighboring tetrahedral, and the fourth is considered non-bridging oxygen (P = O) [60].

It is based on the concept that phosphate glasses are constructed from the number of the building unit (phosphate tetrahedra) to form the structure. The PO_4 unit has three bridging oxygen, which is the Q^3 unit. PO_4 unit with two bridging oxygen is Q^2 unit (metaphosphate). PO_4 unit, which has one bridging oxygen, is Q^1 (pyrophosphate). However, the PO_4 unit with no bridging oxygen is Q^0 (orthophosphate) [61].

The tetrahedral form results from SP^3 hybrid orbitals by outer electrons ($3S^2$, $3P^3$), and the fifth ′e is promoted to the third orbital to form a strong Π bond with oxygen 2P electrons. The tetrahedral links from covalent bridging oxygen can form different phosphate anions. The classification of the different tetrahedral phosphate anions (Q^n) according to BOs can be represented in Ref. [62].

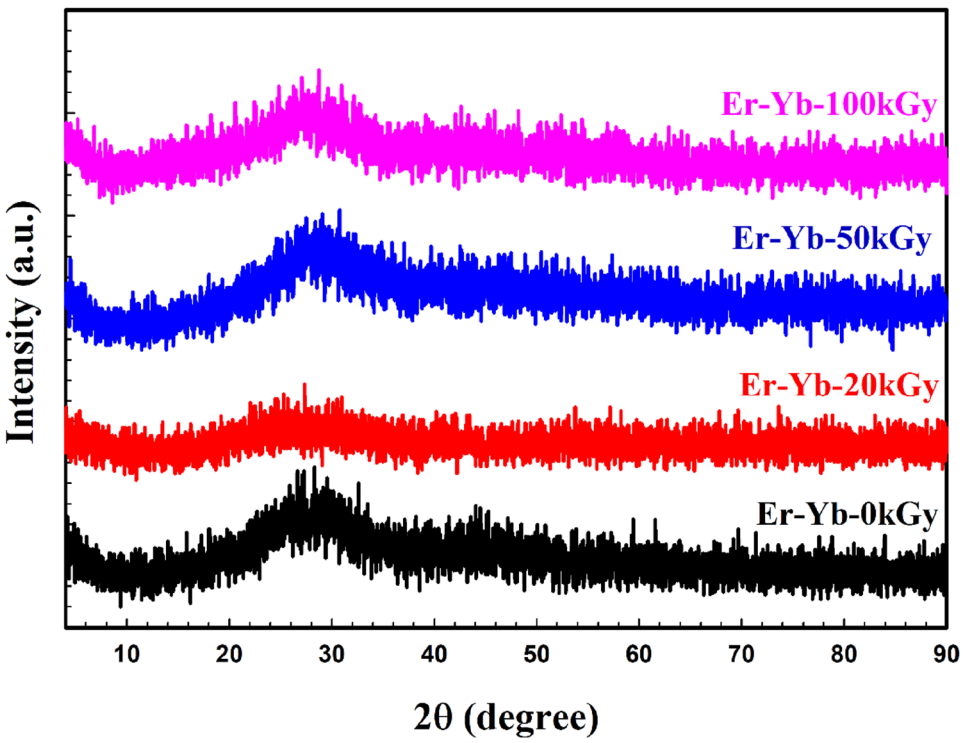

Fig. 1 XRD patterns of Er/Yb-doped lead phosphate glass samples

Figure 2 shows FTIR spectra of Er/Yb-doped lead phosphate glass, whereas Table 1 illustrates the IR absorption peaks assignment for the investigated sample and compares it with other previously prepared phosphate glasses [27, 63, 64]. The spectra show two main areas; one is specific for phosphate groups located in the range from 400 to 1600 cm^{-1}, and the other is specific for OH molecules from 1640 to 4000 cm^{-1}.

Figure 3a–d shows deconvoluted FTIR spectra of Er/Yb-doped lead phosphate glass samples before and

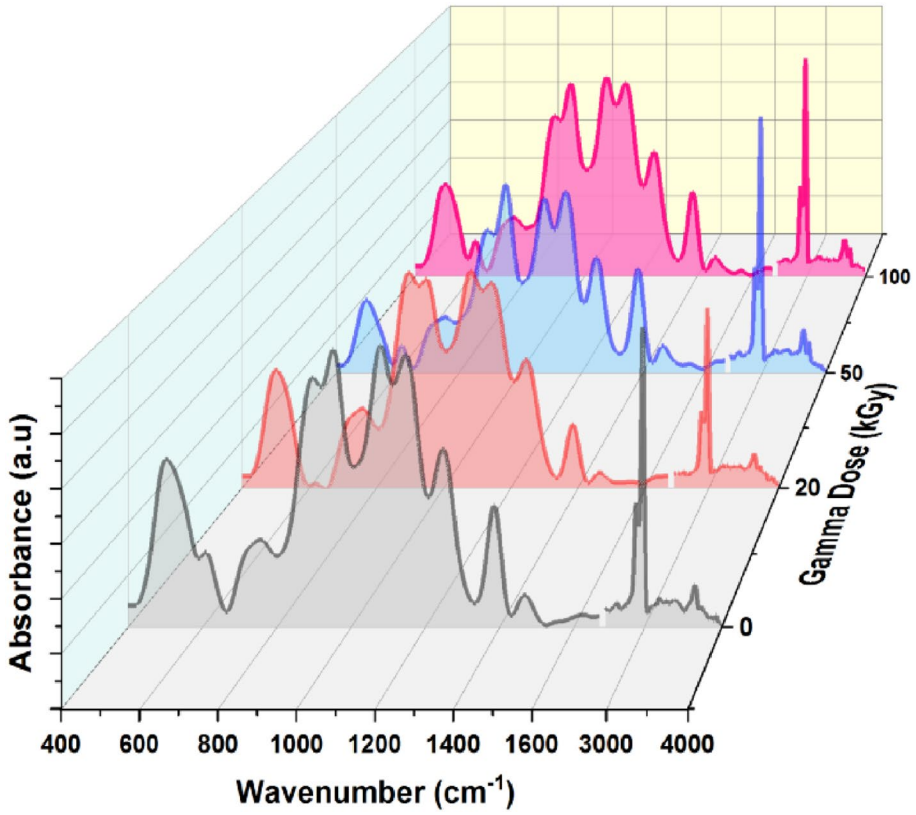

Fig. 2 FTIR spectra of Er/Yb lead phosphate glass samples

Table 1 Assignment of vibrational modes of Er/Yb lead phosphate glass

Vibrational modes	Wavenumber (cm^{-1})			
	Present	[64]	[65]	[27]
Bending of O–P–O	463	475	–	473
Harmonic bending of O = P–O	476	–	–	496
Pb-metaphosphate bond	501	–	500	480
Harmonic bending of P–O–P and for PbO_6 Vib. mode	534	525	–	529
AlO_6 Vib. mode	565	–	–	530
Pb–O and Pb–O–P Vib. from (PbO_4) pyramidal units	617	–	–	640
AlO4 vibration	712	–	–	747
P–O–P $Vib._{sym.}$ for pyrophosphate $(P_2O_7)^{4-}$	764	708	770	770
P–O–P $Vib_{Asym.}$ of bridging oxygen	889	903	875	890
PO_3 $Vib._{sym.}$ and Pb–O from PbO_4	958	900	–	902
PO_3 $Vib._{Asym.}$ of pyrophosphate	1074	1027	1050	1089
O–P–O $Vib._{sym}$	1150	1100	–	1105
P = O $Vib._{Asym.,}$ O–P–O $Vib._{Asym}$	1247	1287	1277	1240
P = O Stretching mode	1383	1390	–	–
P–O–H bridge	1617	1640	–	1695
P–O–H stretching Vib.	2885, 2968	2926	–	2362
H_2O and P–O–H Vib.	3660	3440	–	3619

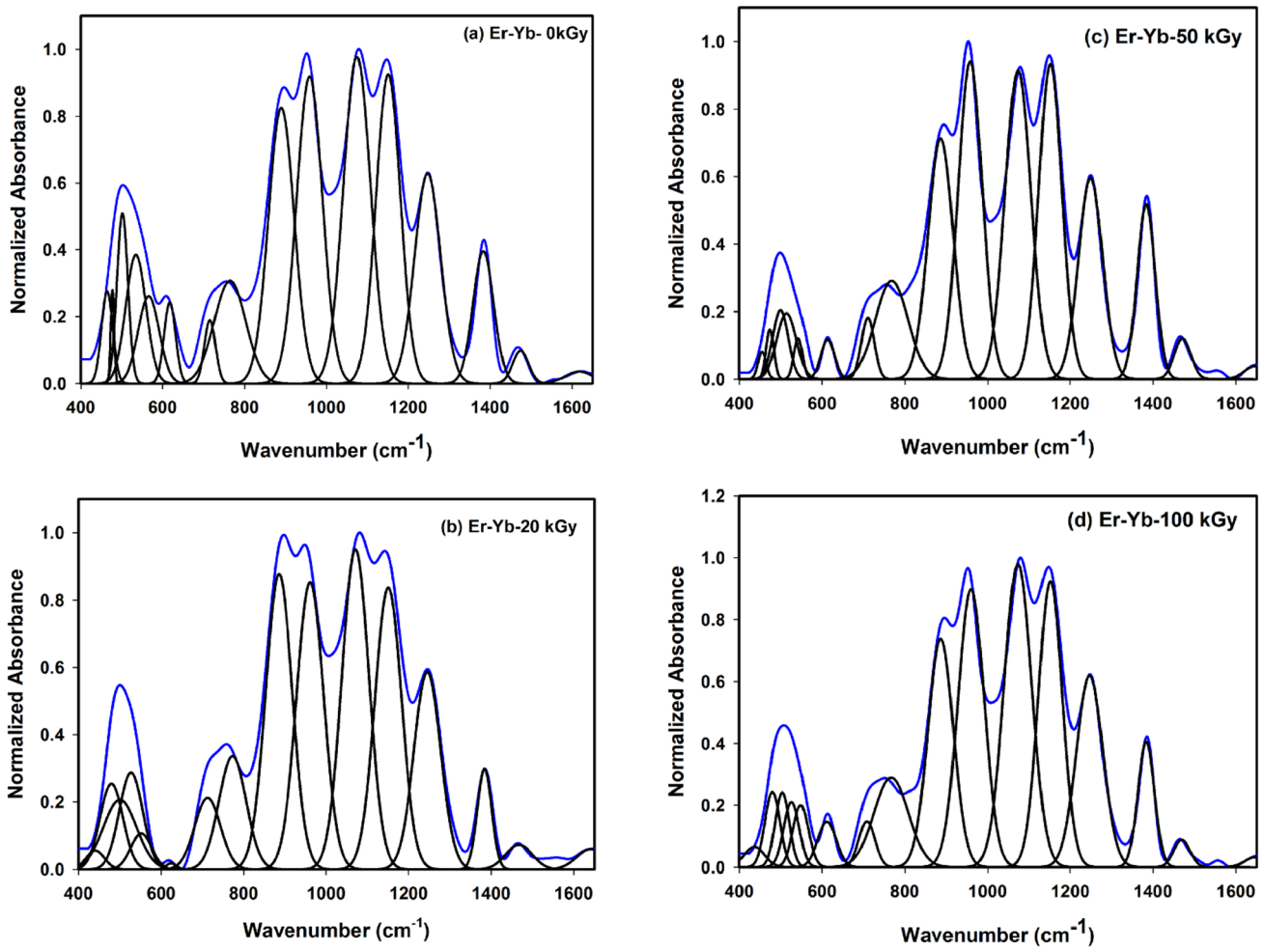

Fig. 3 Deconvoluted FTIR spectra of Er/Yb lead phosphate glass after different gamma irradiated doses: (**a**) 0, (**b**) 20, (**c**) 50, and (**d**) 100 kGy

after irradiation with 20, 50, and 100 kGy. Peaks from 400–590 cm^{-1} give several overlapped peaks at 463, 476, 501, 534, and 564 cm^{-1}, where 463 cm^{-1} is for bending vibrations of O–P–O bond and (PO_2) mode of $(PO_3)^n$ chain [65] and 476 cm^{-1} for harmonic bending of O = P–O of the main phosphate network [66], 501 cm^{-1} is for Pb-metaphosphate bond due to the presence of lead oxide inside the glass network, 534 cm^{-1} is for harmonic bending of P–O–P and PbO_6 vibration mode while 564 cm^{-1} is for AlO_6 group vibration mode [67].

Another peak at 617 cm^{-1} may be related to bonds of Pb–O and Pb–O–P vibration from the formed (PbO_4) pyramidal groups. Also, the extended peak from 710 to 890 cm^{-1} is observed to deconvoluted into three peaks at 712, 764, and 889 cm^{-1}, where the peak at 712 cm^{-1} is for vibration in AlO_4 units as a former oxide, 764 cm^{-1} is for symmetric vibrations of P–O–P bond in pyrophosphate $(P_2O_7)^{4-}$ units and 889 cm^{-1} is considered to be due to the asymmetric vibration of bridging oxygen in P–O–P bonds of different metaphosphate units in the form of a ring, terminal, and chain units.

Two deconvoluted peaks are given at 958 cm^{-1}, associated with symmetric PO_3 and Pb–O from pyramidal groups (PbO_4), while the other is at 1074 cm^{-1} for asymmetrical vibration of PO_3 bonds in pyrophosphate units; this high intensity is due to Na ions. The other two deconvoluted peaks at 1150 cm^{-1} and 1247 cm^{-1} are for symmetrical and asymmetrical O–P–O bonds, respectively. Besides two peaks, one at 1383 cm^{-1} for $(PO_3)^{2-}$ a terminal group that contains the doubly bonded oxygen P = O Stretching mode and 1617 cm^{-1} for the P−O−H bridge. All these peaks are assigned in Table 1. FTIR spectra concluded that the revealed characteristic vibrational bands are related to the presence of metaphosphates (PO^{2-}) and pyrophosphate (PO^{3-}) units, with the first in higher intensity.

In general, FTIR spectra of phosphate glasses are known to have several overlapped peaks, while the position of these peaks can be shifted owing to additives or

Table 2 Deconvolution parameters of the infra-red spectra of studied glasses; band center, relative area, and the amplitude for the samples bands

Peak	Area				Center				Amplitude			
	0 kGy	20 kGy	50 kGy	100 kGy	0 kGy	20 kGy	50 kGy	100 kGy	0 kGy	20 kGy	50 kGy	100 kGy
1	9.53	3.09	2.0	4.1	463.9	440.4	454.9	436.1	0.27	0.06	0.08	0.07
2	2.93	17.6	3.4	10.9	476.9	479.5	473.7	479.7	0.28	0.26	0.15	0.24
3	17.0	20.7	9.7	10.3	501.4	399.9	499.0	503.4	0.51	0.20	0.20	0.24
4	23.9	20.3	11.6	9.9	534.4	526.8	513.6	525.6	0.38	0.29	0.19	0.21
5	16.8	6.7	3.2	9.5	565.7	551.4	541.9	547.9	0.26	0.11	0.12	0.19
6	8.5	0.57	4.8	8.3	617.5	624.9	613.4	611.4	0.24	0.02	0.12	0.15
7	6.3	16.5	7.1	7.3	715.4	712.6	710.4	707.9	0.19	0.21	0.18	0.15
8	29.5	27.7	28.9	30.2	764.1	772.9	767.9	766.7	0.30	0.34	0.29	0.29
9	65.2	70.9	54.5	56.5	889.5	885.4	886.2	886.3	0.83	0.87	0.71	0.74
10	72.7	70.1	68.6	70.9	958.8	961.2	967.7	959.8	0.92	0.85	0.94	0.89
11	80.5	77.9	71.8	81.8	1074.6	1070.9	1073.5	1073.2	0.98	0.95	0.91	0.98
12	69.1	67.5	65.6	66.6	1150.8	1150.3	1151.7	1151.8	0.92	0.84	0.93	0.92
13	50.4	47.5	43.6	49.9	1247.2	1245.4	1248.8	1246.6	0.63	0.58	0.59	0.62
14	25.4	21.8	28.5	20.4	1383.5	1383.6	1383.3	1383.3	0.39	0.29	0.52	0.41
15	2.7	4.63	2.89	2.29	1617.03	1641.32	1647.31	1647.25	0.04	0.06	0.39	0.33

the composition of the glass, as given in Table 2. Various induced defects have been detected relying on the intensity of radiation exposure and charged particle irradiation [68, 69]. Glasses often have a limited range of orders and suffer from defect sites. Suppose the energy of the photon is greater than the bandgap. In that case, electrons are liberated from the valence band, and the remaining energy will be transferred to kinetic energy if the glasses are irradiated to electromagnetic fields [68]. Consequently, the escaped electrons migrate through the glass network. They are either captured via pre-existing defects for generating induced defect centers in the glasses or generate secondary electron cascades through knock-on collision with the bound electrons throughout the terms of excess energy Compton electrons. The major vibrated groups appeared in almost the same numbers and positions upon irradiation to various gamma doses as they achieved in the non-treated sample. It reveals that the total phosphate structural units (metaphosphate (PO^{2-}) and pyrophosphate (PO^{3-})) units of the investigated glasses continue to stay in overall with their arrangement typically [70]. The reduction in pyrophosphate groups and the corresponding rise in metaphosphate groups might be ascribed to the decrease in the peak intensity at 1074 cm^{-1} after progressive gamma irradiation doses. In addition, the shift of the peaks, which matched with a decrease in intensity at 764 cm^{-1} upon irradiation with different gamma doses, may be due to a change in bond angles besides the change in the bond length of the P–O–P bridges which means the glass network stability against radiation [64, 71–73]. Also, decreasing the intensity of the peaks in the area of 600–650 cm^{-1} and 900–1200 cm^{-1} may be attributed to the rearrangement of defects and NBO originated by irradiation that resulted in conversion from PO_4 (tetrahedral groups) to PO_3 units [5].

5 Linear optical properties

5.1 The absorption spectra behavior

The absorption spectra of Er–Yb lead phosphate glass samples are shown in Fig. 4. For the pristine glass sample (0 kGy), the absorption bands can be categorized into three mean regions; the first one is located in the range of 190–300 nm for the oxygen deficient center (ODC), which depends on the existence

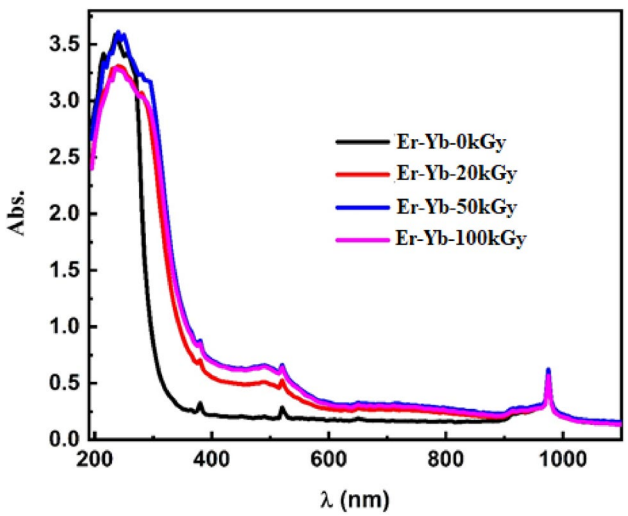

Fig. 4 Absorbance spectra of Er–Yb lead phosphate glass samples

of P, Pb, and Al within the matrix. Along with the presence of Yb^{2+} and other non-bridging oxygen hole centers (NBOC), this region is believed to be responsible for the photodarkening effect (PD) in optical amplifier glasses. Second region; show small bands at about 378 and 522 nm were assigned to transitions from ground-state $4I_{15/2}$ to $2H_{7/2}$ and $4F_{9/2}$ excited states of Er^{3+}. The last region is for absorption peak at ~ 978 nm is ascribed to $(2F_{7/2} \rightarrow 2F_{5/2})$ of Yb^{3+} [74–77]. In general, irradiation causes the electrons that are already present in the glass matrix to get excited, and these excited electrons have the potential to eject themselves in accordance with the dosage, therefore, increasing the number of NBOs. Irradiation causes some of these electrons to get excited, and some of those electrons may be utilised to heal defects that are already present in the glass matrix. But in the other hand, Yb ions have the ability to captivate these electrons in during charge transfer (CT) process between Yb and Er, which will also assist in returning some of the NBOs to the BOs and beginning to form more covalent bonds between the cations and the O^{2-} as observed by a reduction in the intensity of the bands with a small lower shift in the wavelength in the first region upon 20 and 100 kGy. The second and third areas do not produce any shift in the wavelength; rather, a rise in the band intensities is the only change that can be seen.

5.2 The spectral distribution of absorption index

The extinction coefficient (k) can be deduced as a function of the absorbance coefficient α (λ) [78–80].

$$k = \frac{\alpha\lambda}{4\pi} \tag{1}$$

The extinction coefficient (k) spectra of Er/Yb lead phosphate glass samples are presented in Fig. 5. The spectral behavior of k has been observed to be influenced by gamma dosages. Irradiation of Er/Yb lead phosphate glass decreases the absorption index but has little effect on the spectra' peak position of absorption bands. Also, it is worth noting that the value of k has never approached zero. This behavior might be considered a unique feature of free carriers' appearances.

5.3 The refractive index spectra (n)

The refractive index (n), which is controlled by the interaction of light with the electrons of the component atoms of the glass, is another essential characteristic of the optoelectronic properties of the studied glass. It is influence by oxides in the glass sample, cationic polarizability, and radiation doses. The rise in NBOs, created due to the effect of gamma radiation, increases the refractive indices of a standard glass system.

The following expression can derive the refractive index (n) of Er/Yb lead phosphate glass samples [78–80].

$$n = \frac{1+R}{1-R} + \sqrt{\frac{4R}{(1-R)^2} - k^2} \tag{2}$$

The spectra of the refractive index, n, for Er/Yb lead phosphate glass samples are seen in Fig. 6. We found that the value of n changes slightly after irradiation in all wavelength ranges. Also, the absorption peaks were shifted to higher wavelengths with increasing gamma radiation doses.

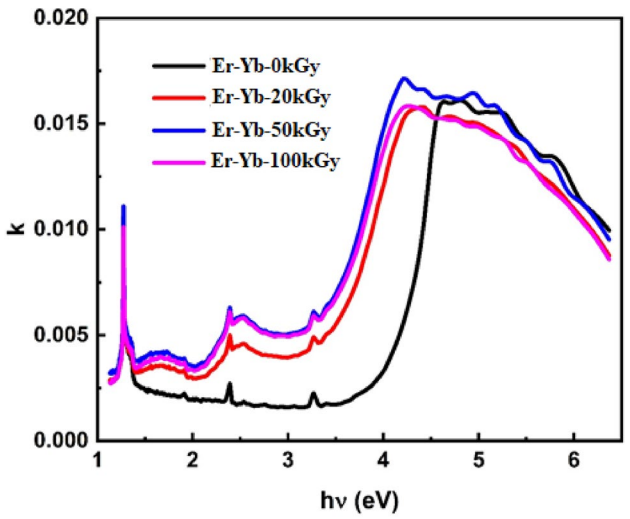

Fig. 5 The extinction coefficient (k) spectra of Er/Yb lead phosphate glass samples

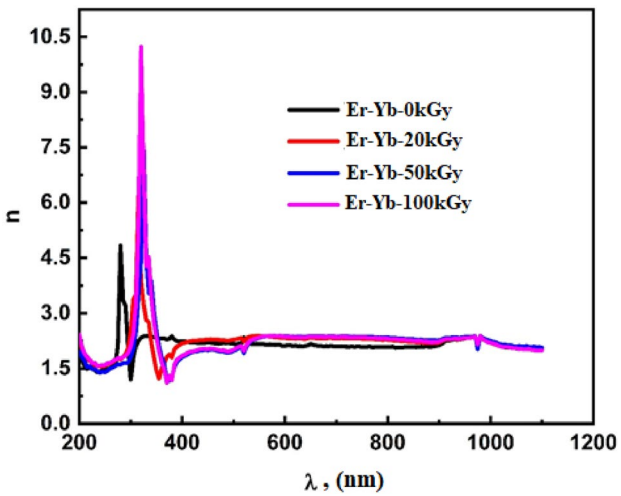

Fig. 6 The refractive index spectra, n, of Er/Yb lead phosphate glass samples.

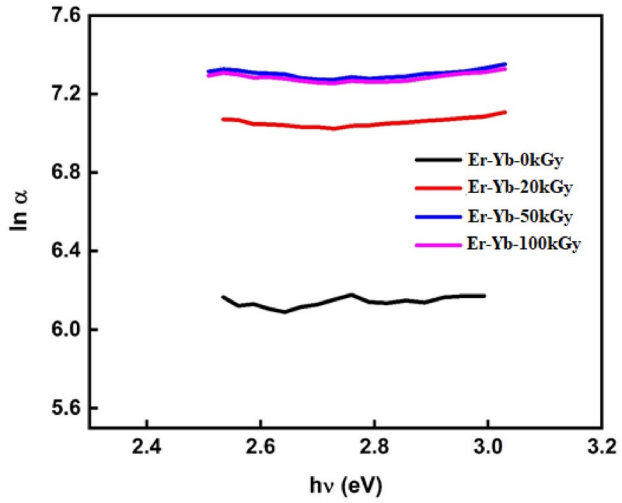

Fig. 7 Plot of Ln(α) vs. (hν) for Er/Yb lead phosphate glass samples.

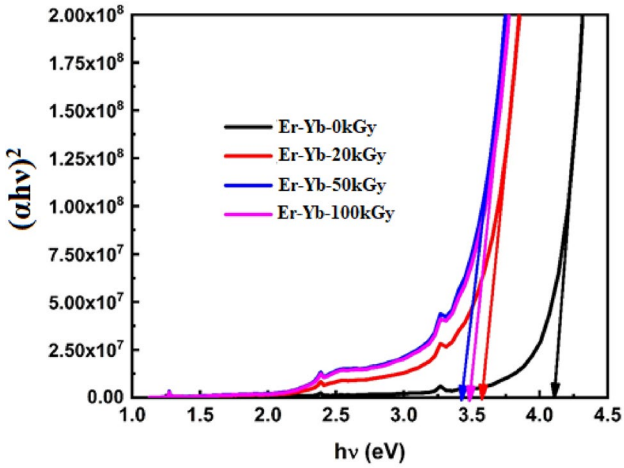

Fig. 8 $(\alpha h\nu)^2$ vs. (hν) for Er/Yb lead phosphate glass samples

5.4 Urbach and optical bandgap energies

The Urbach energy, Eu, may be derived in the low incident photons energy spectrum through graphing the relationship between lnα and hν (see Fig. 7) [81]:

$$\ln \alpha = \ln \alpha_0 + \frac{h\nu}{E_u} \tag{3}$$

The Urbach energy (E_u) values of Er/Yb lead phosphate glass samples are summarized and tabulated in Table 3. We will see that enhanced doses of up to 50 kGy improve the Urbach energy of Er/Yb lead phosphate glass samples and then declines at a dose of 100 kGy. That means the increase in the depolymerization of the glassy network up to 50 kGy making the glass samples less compacted due to more formation of NBOs amount. The Eu of Er/Yb lead phosphate glass samples increases from 10.23 eV for the pristine glass sample to 37.03 eV at 50 kGy.

Using the Tauc relation, the optical band gap energy of Er/Yb lead phosphate glass samples was related to α and $h\nu$[82]:

$$\alpha h\nu = A(h\nu - E_g)^t, \tag{4}$$

Table 3 The optical bandgap E_g, Urbach energy E_u, and the dispersion parameters for the Er/Yb lead phosphate glass samples

Sample	E_g (eV)	E_u (eV)	E_0 (eV)	E_d (eV)	ε_∞
0 kGy	4.11	10.23	1.56	2.21	2.41
20 kGy	3.56	12.70	1.59	2.37	2.48
50 kGy	3.42	37.03	1.62	2.71	2.66
100 kGy	3.48	33.55	1.55	2.11	2.36

in which A is a constant, t denotes the transition type, and E_g represents the energy gap

As shown in Fig. 8, the direct optical band gap energy, E_g, may be calculated by graphing $(\alpha h\nu)^2$ as a function of (hν) for Er/Yb lead phosphate glass samples. Table 3 lists the values of the energy band gaps for direct transitions. We note that by increasing the irradiation doses up to 50 kGy, a decrease in the energy gap was observed and then increased at the dose of 100 kGy. The direct optical band gap energy decreased from 4.11 eV for pristine Er/Yb lead phosphate glass to 3.42 eV at 50 kGy. These results agree with previous findings of Urbach's energy behavior. That may explained as by increasing gamma doses, the amount of created excited electrons and non-bridging oxygen increased and moved through the already excited defects inside lead phosphate glass sample that act as tunnels between energy levels till reach 100 kGy where the excited electrons being to be captured by converting NBOs to BO that reduce the amount of net empty defects.

A material's optical density (Dopt) is related to its thickness and absorption coefficient. The present glass system's optical density (Dopt) may be computed using the formula below [34]:

$$D_{opt} = \alpha(v)r, \tag{5}$$

in which, r is the thickness of the sample.

Figure 9 illustrates the optical density (D_{opt}) spectrum of Er/Yb lead phosphate glass samples. The optical density of the synthetic glass rises as gamma radiation exposures rise. This rise caused the wide near-visible band to shift in the direction of a higher wavelength, which was generated by a reduction in the bandgap.

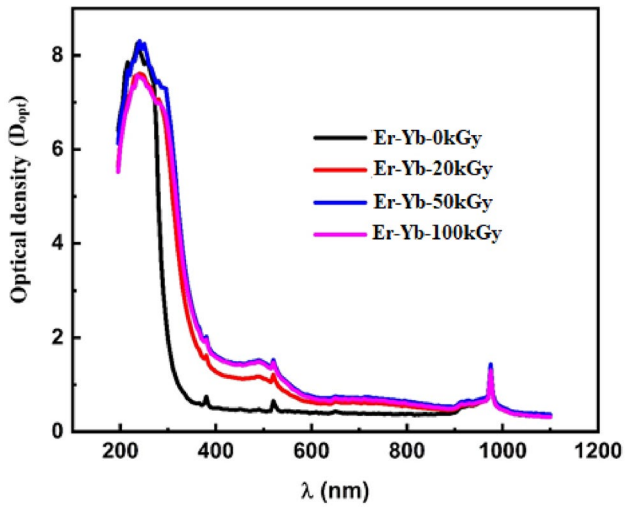

Fig. 9 The optical density (D_{opt}) spectrum of Er/Yb lead phosphate glass samples

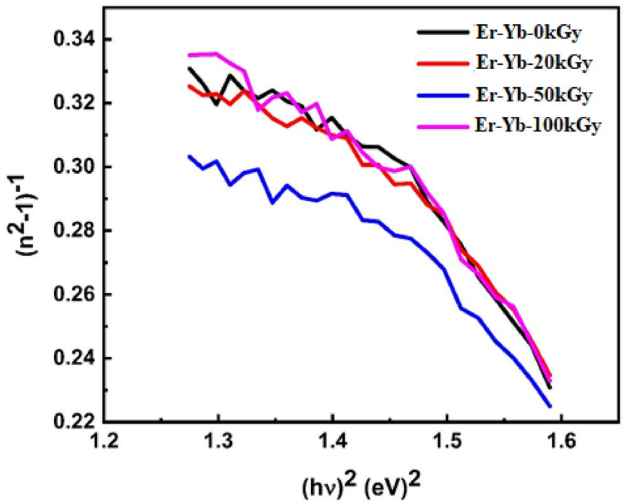

Fig. 10 $(n^2-1)^{-1}$ vs. $(h\nu)^2$ for Er/Yb lead phosphate glass samples

5.5 Dispersion and the dielectric performance

The dispersion behavior plays a very important role in assessing optical materials since it is a vital factor in optical communication and the manufacturing of spectral dispersion technologies.

The single oscillator model could be used to calculate the oscillator energy E_o, dispersion energy E_d, and static dielectric constant ($\varepsilon_\infty = n^2$) for Er/Yb lead phosphate glass samples, which can then be expressed using Wemple and DiDomenico formula [83].

The relationship between $(n^2-1)^{-1}$ and $(h\nu)^2$ for Er/Yb lead phosphate glass samples is seen in Fig. 10. Table 3

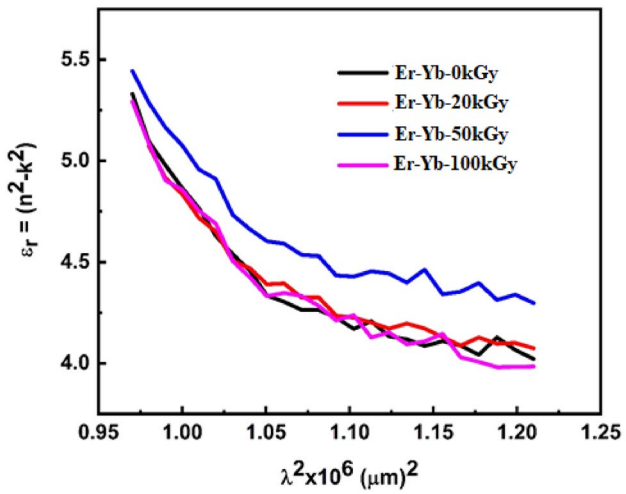

Fig. 11 (n^2-k^2) vs. λ^2 for Er/Yb lead phosphate glass samples

Table 4 The free carrier concentration (N), (N/m*), and the lattice dielectric constant (ε_l) for Er/Yb lead phosphate glass samples

Sample	N/m* (cm^3/g)	N (cm^3)	ε_L
0 kGy	4.86×10^{47}	4.4×10^{20}	5.54
20 kGy	5.29×10^{47}	4.8×10^{20}	5.71
50 kGy	4.82×10^{47}	4.3×10^{20}	5.81
100 kGy	8.66×10^{47}	7.8×10^{20}	6.63

validates the (E_o, E_d, and ε_∞) values. Increased the irradiated dosages up to 50 kGy resulted in a significant rise in these values, which subsequently reduced at 100 kGy. The oscillator energy Eo was found between 1.55 to 1.62 eV. Also, the dispersion energy E_d ranged from 2.11 eV at 100 kGy to 2.71 eV at the dose of 50 kGy. We observed that the dispersion constants values had been empirically related to the bandgap variation [84]. Also, the static dielectric constant varied between 2.36 and 2.66.

The percentage of free carrier ions to effective mass (N/m*) is reliant on the lattice dielectric constant (ε), wavelength λ, and the refractive index [85]:

$$n^2 - k^2 = \varepsilon_l - \left(\frac{e^2}{4\pi^2\varepsilon_0 c^2}\right)\left(\frac{N}{m^*}\right)\lambda^2. \quad (6)$$

The relationship between (n^2-k^2) vs. λ^2 for Er/Yb lead phosphate glass samples is seen in Fig. 11. Table 4 lists the values for these parameters. The percentage of free carrier ions to effective mass (N/m*) increased with increasing gamma doses but declined at 50 kGy, where the N/m* values in the range $(4.82–8.66)\times10^{47}$ cm^3/g. Besides, the lattice dielectric constant (ε_l) increased from 5.54 to 6.63 with increasing the gamma doses.

6 Nonlinear optical properties

The following expression was used to compute the nonlinear third-order optical susceptibility ($\chi^{(3)}$) for Er/Yb lead phosphate glass samples using linear refractive index and dispersion parameters (E_o and Ed) [86–88]:

$$\chi^{(3)} = A\left(\frac{E_o E_d}{4\pi(E_o^2 - (h\nu)^2}\right)^4, \tag{7}$$

where $A \sim 1.7 \times 10^{-10}$ esu [89].

The relationship between $\chi^{(3)}$ and $h\nu$ for Er/Yb lead phosphate glass samples is shown in Fig. 12. The susceptibility $\chi^{(3)}$ is the outcome of the Er/Yb lead phosphate glass samples reaction to the impacted electric field of light. We can see from Fig. 12 that increasing gamma doses up to 50 kGy enhances the susceptibility $\chi^{(3)}$ and then reduces at 100 kGy, so we assume that the increase of gamma doses beyond 50 kGy reduces polarizability ability. The electrical polarizability of the irradiated Er/Yb lead phosphate glass samples opens up the prospect of using them in optoelectronics applications.

Figure 13 demonstrates the correlation between the nonlinear refractive index and λ for Er/Yb lead phosphate glass samples. The nonlinear susceptibility can be used to calculate the nonlinear refractive index, n_2, using the formula [86, 87]:

$$n_2 = \frac{12\pi\chi^{(3)}}{n_o}. \tag{8}$$

We can see that from Fig. 13 that increasing gamma doses up to 50 kGy reduces the nonlinear refractive index, n_2, and then improves at 100 kGy,

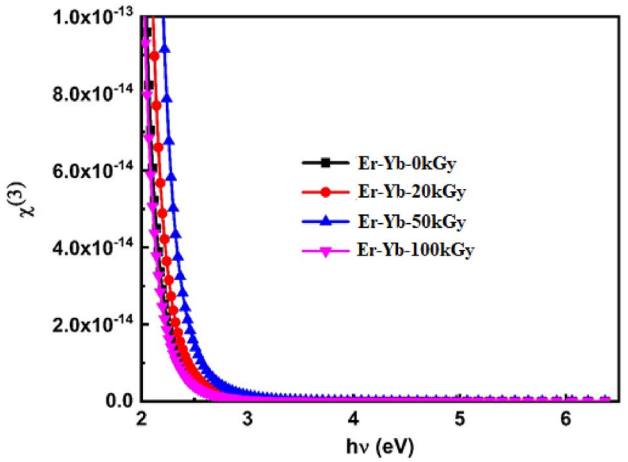

Fig. 12 The relationship between $\chi^{(3)}$ and $h\nu$ for Er/Yb lead phosphate glass samples

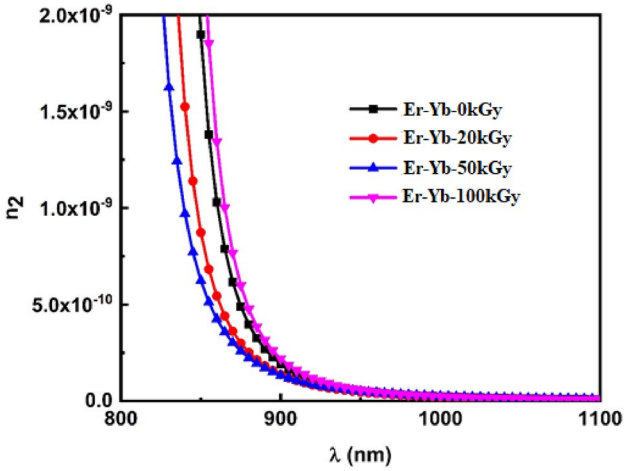

Fig. 13 The correlation between the nonlinear refractive index n_2 and λ for Er/Yb lead phosphate glass samples

The nonlinear absorption coefficient β_C spectra for Er/Yb lead phosphate glass samples were based on their band structure. It controls the energy states and may well be derived using the formula [86, 87]:

$$\beta_c = \frac{K_c E_p^{1/2} F}{n^2 E_g^3}, \tag{9}$$

$$F = \frac{\left(\frac{2h\nu}{E_g} - 1\right)^{3/2}}{(2h\nu/E_g)^5}. \tag{10}$$

K_c is constant (3100 cm/GW), Ep is the Kane energy, and the dispersion of absorption coefficient is denoted by F, which is related to photon energy. The nonlinear absorption coefficient β_C varied as the gamma doses enhanced (Fig. 14).

7 Conclusion

The purpose of this study was to reveal the effect of gamma rays on the Er/Yb lead phosphate glass system's physical, structural, linear, and nonlinear optical characteristics. The Er/Yb lead phosphate glass's amorphous nature was verified using XRD patterns. FTIR spectra likewise reveal the resistance of Er/Yb lead phosphate glass against radiation with slight adjustments in the intensities of specific bands. The Eu value of Er/Yb lead phosphate glass samples increases from 10.23 eV for the pristine glass sample to 37.03 eV at 50 kGy. Also, the direct optical band gap energy decreased from 4.11 eV for pristine Er/Yb lead phosphate glass to 3.42 eV at 50 kGy. The

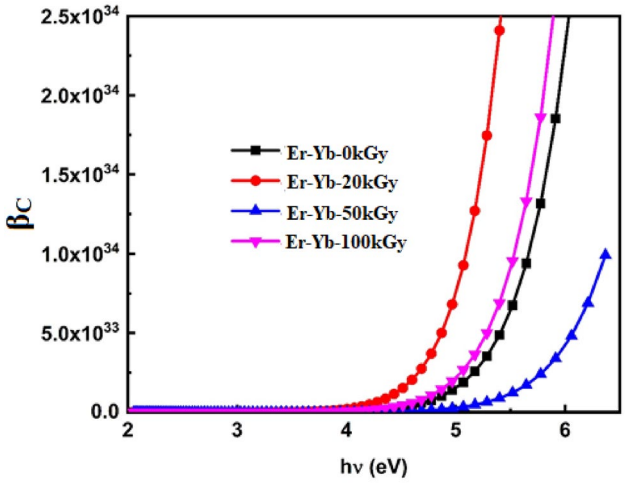

Fig. 14 The nonlinear absorption coefficient β_C spectra for Er/Yb lead phosphate glass samples

oscillator energy *E*o was found between 1.55 and 1.62 eV. Also, the dispersion energy E_d ranged from 2.11 eV at 100 kGy to 2.71 eV at the dose of 50 kGy. The free carrier concentration (N) increased with increasing gamma doses but declined at 50 kGy, where the percentage of free carrier ions to effective mass (N/m*) values in the range $(4.82–8.66) \times 10^{47}$ cm^3/g. Besides, the lattice dielectric constant (ε_l) increased from 5.54 to 6.63 with increasing the gamma doses. Furthermore, increasing gamma doses up to 50 kGy enhances the susceptibility $\chi^{(3)}$ and then reduces at 100 kGy, assuming that increasing gamma doses beyond 50 kGy reduces polarizability ability. While the increasing gamma doses up to 50 kGy reduces the nonlinear refractive index and then improves at 100 kGy. Altogether, the nonlinear and linear findings demonstrate that Er/Yb lead phosphate glass could be a potential candidate for optical applications such as gain media and optical amplifiers.

Funding Open access funding provided by The Science, Technology & Innovation Funding Authority (STDF) in cooperation with The Egyptian Knowledge Bank (EKB).

Declarations

Conflict of interest The authors declare that they have no conflict of interest.

References

1. P. Ramesh, V. Hegde, K. Keshavamurthy, A. Pramod, G. Jagannath, D.A. Aloraini, A.H. Almuqrin, M. Sayyed, K. Harisha, S. Khan, Influence of gamma irradiation on photoluminescence and nonlinear optical properties of Eu3+ activated heavy metal borate glasses. Opt. Mater. **116**, 111102 (2021)
2. A. Górny, M. Sołtys, J. Pisarska, W.A. Pisarski, Effect of acceptor ions concentration in lead phosphate glasses co-doped with Tb3+–Ln3+ (Ln= Eu, Sm) for LED applications. J. Rare Earths **37**(11), 1145–1151 (2019)
3. M. Norkus, M. Skruodienė, G. Niaura, A. Šarakovskis, R. Skaudžius, New low-temperature phosphate glasses as a host for Europium Ions. J. Non-Cryst. Solids **569**, 120966 (2021)
4. S. Mohan, S. Kaur, P. Kaur, D. Singh, Spectroscopic investigations of Sm3+-doped lead alumino-borate glasses containing zinc, lithium and barium oxides. J. Alloy. Compd. **763**, 486–495 (2018)
5. O. Sallam, A. Abdeldaym, F. Ezz-Eldin, Synthesis and physical characterization of gamma irradiated cadmium phosphate glass modified by copper oxide. Mater. Chem. Phys. **252**, 123241 (2020)
6. A.H.D. Prakash, S. Mahamuda, J.S. Alzahrani, P. Sailaja, K. Swapna, M. Venkateswarlu, A. Rao, Z. Alrowaili, I. Olarinoye, M. Al-Buriahi, Synthesis and characterization of B2O3–Bi2O3–SrO–Al2O3–PbO–Dy2O3 glass system: The role of Bi2O3/Dy2O3 on the optical, structural, and radiation absorption parameters. Mater. Res. Bull. **155**, 111952 (2022)
7. Z.A. Alrowaili, A.M. Ali, A.M. Al-Baradi, M.S. Al-Buriahi, E.A.A. Wahab, K.S. Shaaban, A significant role of MoO3 on the optical, thermal, and radiation shielding characteristics of B2O3–P2O5–Li2O glasses. Opt. Quant. Electron. **54**(2), 88 (2022)
8. J.S. Alzahrani, A. Sharma, S.N. Nazrin, Z.A. Alrowaili, M.S. Al-Buriahi, Optical and radiation shielding effectiveness of a newly fabricated WO3 doped TeO2–B2O3 glass system. Radiat. Phys. Chem. **193**, 109968 (2022)
9. J.S. Alzahrani, Z. Alrowaili, H. Saleh, A. Hammoud, S. Alomairy, C. Sriwunkum, M. Al-Buriahi, Synthesis, physical and nuclear shielding properties of novel Pb–Al alloys. Prog. Nucl. Energy **142**, 103992 (2021)
10. M. Al-Buriahi, M. Hessien, F. Alresheedi, A.M. Al-Baradi, Z. Alrowaili, I. Kebaili, I. Olarinoye, ZnO–Bi2O3 nanopowders: Fabrication, structural, optical, and radiation shielding properties. Ceram. Int. **48**(3), 3464–3472 (2022)
11. Z. Alrowaili, T. Taha, M. Ibrahim, K. Saron, C. Sriwunkum, A.M. Al-Baradi, M. Al-Buriahi, Synthesis and characterization of B2O3-Ag3PO4-ZnO-Na2O glasses for optical and radiation shielding applications. Optik **248**, 168199 (2021)
12. P.R. Rani, M. Venkateswarlu, S. Mahamuda, K. Swapna, N. Deopa, A. Rao, G.V. Prakash, Structural, absorption and photoluminescence studies of Sm3+ ions doped barium lead alumino fluoro borate glasses for optoelectronic device applications. Mater. Res. Bull. **110**, 159–168 (2019)

13. M. Zagrai, R.-C. Suciu, S. Rada, M. Pică, S. Pruneanu, Structural and optical properties of Eu3+ ions in lead glass for photonic applications. J. Non-Cryst. Solids **569**, 120988 (2021)
14. M. Marzouk, H. Elbatal, Investigation of photoluminescence and spectroscopic properties of Sm 3+-doped heavy phosphate glasses before and after gamma irradiation. Appl. Phys. A **127**(1), 1–10 (2021)
15. S. Damodaraiah, V.R. Prasad, R.V. Lakshmi, Y. Ratnakaram, Luminescence behaviour and phonon sideband analysis of europium doped Bi2O3 based phosphate glasses for red emitting device applications. Opt. Mater. **92**, 352–358 (2019)
16. D. Shajan, P. Murugasen, S. Sagadevan, Studies on structural, optical and spectral properties of Europium oxide doped phosphate glasses. Optik **136**, 165–171 (2017)
17. C. Nico, R. Fernandes, M. Graça, M. Elisa, B. Sava, R. Monteiro, L. Rino, T. Monteiro, Eu3+ luminescence in aluminophosphate glasses. J. Lumin. **145**, 582–587 (2014)
18. A. Langar, C. Bouzidi, H. Elhouichet, B. Gelloz, M. Ferid, Investigation of spectroscopic properties of Sm-Eu codoped phosphate glasses. Displays **48**, 61–67 (2017)
19. C. Basavapoornima, C. Kesavulu, T. Maheswari, W. Pecharapa, S.R. Depuru, C. Jayasankar, Spectral characteristics of Pr3+-doped lead based phosphate glasses for optical display device applications. J. Lumin. **228**, 117585 (2020)
20. K. Kirdsiri, R. Rajaramakrishna, B. Damdee, H. Kim, N. Nuntawong, M. Horphathum, J. Kaewkhao, Influence of alkaline earth oxides on Eu3+ doped lithium borate glasses for photonic, laser and radiation detection material applications. Solid State Sci. **89**, 57–66 (2019)
21. N. Deopa, S. Kaur, A. Prasad, B. Joshi, A. Rao, Spectral studies of Eu3+ doped lithium lead alumino borate glasses for visible photonic applications. Opt. Laser Technol. **108**, 434–440 (2018)
22. M. Sołtys, J. Janek, L. Żur, J. Pisarska, W.A. Pisarski, Compositional-dependent europium-doped lead phosphate glasses and their spectroscopic properties. Opt. Mater. **40**, 91–96 (2015)
23. N. Chanthima, Y. Tariwong, H.J. Kim, J. Kaewkhao, N. Sangwaranatee, *Effect of Eu3+ Ions on the Physical* (Key Engineering Materials, Trans Tech Publ, Optical and Luminescence Properties of Aluminium Phosphate Glasses, 2018), pp.122–126
24. S.S. Babu, P. Babu, C. Jayasankar, A. Joshi, A. Speghini, M. Bettinelli, Laser transition characteristics of Nd3+-doped fluorophosphate laser glasses. J. Non-Cryst. Solids **353**(13–15), 1402–1406 (2007)
25. W.A. Pisarski, Ł Grobelny, J. Pisarska, R. Lisiecki, W. Ryba-Romanowski, Spectroscopic properties of Yb3+ and Er3+ ions in heavy metal glasses. J. Alloy. Compd. **509**(31), 8088–8092 (2011)
26. K. Naseer, K. Marimuthu, The impact of Er/Yb co-doping on the spectroscopic performance of bismuth borophosphate glasses for photonic applications. Vacuum **183**, 109788 (2021)
27. N. El-Alaily, O. Sallam, F. Ezz-Eldin, Effect of gamma irradiation on some spectroscopic properties of phosphate glass containing samarium ions. J. Non-Cryst. Solids **523**, 119604 (2019)
28. E. Snitzer, R. Woodcock, Yb3+–Er3+ GLASS LASER. Appl. Phys. Lett. **6**(3), 45–46 (1965)
29. E. Snitzer, H. Po, F. Hakimi, R. Tumminelli, B. McCollum, 1988 ERBIUM FIBER LASER AMPLIFIER AT 1.55 μm WITH PUMP AT 1.49 μm AMD Yb SENSITIZED Er OSCILLATOR, Optical Fiber Communication Conference, Optical Society of America, p. PD2
30. N. Elalaily, A. Zahran, E. Saad, O. Sallam, F. Ezz-Eldin, Corrosion and infrared study of some γ-irradiated lead-phosphate glasses doped with MoO 3. SILICON **10**(4), 1613–1623 (2018)
31. C. Venkateswarlu, M. Seshadri, Y. Ratnakaram, Influence of mixed alkalis on spectroscopic parameters of Sm3+, Dy3+ doped chloroborate glasses. Opt. Mater. **33**(6), 799–806 (2011)
32. A. Ibrahim, A.H. Hammad, A. Abdelghany, G. Rabie, Mixed alkali effect and samarium ions effectiveness on the structural, optical and non-linear optical properties of borate glass. J. Non-Cryst. Solids **495**, 67–74 (2018)
33. D. Ehrt, Photoluminescence in the UV–VIS region of polyvalent ions in glasses. J. Non-Cryst. Solids **348**, 22–29 (2004)
34. S.M. Kassem, G. Ahmed, A. Rashad, S. Salem, S. Ebraheem, A. Mostafa, An investigation of the nuclear shielding effectiveness of some transparent glasses manufactured from natural quartz doped lead cations. Nucl. Eng. Technol. **53**(6), 2025–2037 (2021)
35. J.E. Shelby, Introduction to glass science and technology, Royal Society of Chemistry2020
36. F. ElBatal, M. Marzouk, Gamma rays interaction with bismuth borate glasses doped by transition metal ions. J. Mater. Sci. **46**(15), 5140–5152 (2011)
37. N. Elalaily, R. Mahamed, Effects of fast neutron and gamma irradiation on electrical conductivity of some borate glasses. J. Nucl. Mater. **303**(1), 44–51 (2002)
38. G. Okada, S. Kasap, T. Yanagida, Optically-and thermally-stimulated luminescences of Ce-doped SiO2 glasses prepared by spark plasma sintering. Opt. Mater. **61**, 15–20 (2016)
39. P. Ramesh, V. Hegde, A. Pramod, B. Eraiah, D. Agarkov, G. Eliseeva, M. Pandey, K. Annapurna, G. Jagannath, M. Kokila, Compositional dependence of red photoluminescence of Eu3+ ions in lead and bismuth containing borate glasses. Solid State Sci. **107**, 106360 (2020)
40. T. Kuro, G. Okada, N. Kawaguchi, Y. Fujimoto, H. Masai, T. Yanagida, Scintillation properties of rare-earth doped NaPO3-Al (PO3) 3 glasses. Opt. Mater. **62**, 561–568 (2016)
41. S. Girard, M. Vivona, A. Laurent, B. Cadier, C. Marcandella, T. Robin, E. Pinsard, A. Boukenter, Y. Ouerdane, Radiation hardening techniques for Er/Yb doped optical fibers and amplifiers for space application. Opt. Express **20**(8), 8457–8465 (2012)
42. M.I.A. Abdel Maksoud, S.M. Kassem, O.I. Sallam, (2022) Structural, optical, and radiation shielding features of newly developed BaZrO3/Na2O–B2O3 glass, Ceramics International
43. M.I.A. Abdel Maksoud, O.I. Sallam, S.M. Kassem, R.A. Fahim, A.S. (2022) Awed, Novel Strategy for Hazardous Cement Bypass Dust Removal: Structural, Optical and Nuclear Radiation Shielding Properties of CBD-Bismuth Borate Glass. Journal of Inorganic and Organometallic Polymers and Materials
44. E.K. Abdel-Khalek, D.A. Rayan, A.A. Askar, M.I.A.A. Maksoud, H.H. El-Bahnasawy, Synthesis and characterization of SrFeO3-δ nanoparticles as antimicrobial agent. J. Sol-Gel. Sci. Technol. **97**(1), 27–38 (2021)
45. A.S. Awed, M.I.A.A. Maksoud, M.M. Atta, R.A. Fahim, Nonlinear optical properties of irradiated 1,2-dihydroxyanthraquinone thin films: merged experimental and TD-DFT insights. J. Mater. Sci.: Mater. Electron. **30**(8), 7858–7865 (2019)
46. M.A. Maksoud, M.M. Ghobashy, G.S. El-Sayyad, A.M. El-Khawaga, M.A. Elsayed, A. Ashour, Gamma irradiation-assisted synthesis of PANi/Ag/MoS2/LiCo0. 5Fe2O4 nanocomposite: Efficiency evaluation of photocatalytic bisphenol A degradation and microbial decontamination from wastewater. Opt. Mater. **119**, 111396 (2021)
47. M. Abdel Maksoud, A. El-Ghandour, G.S. El-Sayyad, R.A. Fahim, A.H. El-Hanbaly, M. Bekhit, E. Abdel-Khalek, H. El-Bahnasawy, M. Abd Elkodous, A. Ashour, Unveiling the effect of Zn2+ substitution in enrichment of structural, magnetic, and dielectric properties of cobalt ferrite. J. Inorg. Organomet. Polym Mater. **30**(9), 3709–3721 (2020)

48. M. Maksoud, G.S. El-Sayyad, M. Abd El-Kodous, A., Awed, Controllable synthesis of Co1-x MxFe2O4 nanoparticles (M= Zn, Cu, and Mn; x= 0.0 and 0.5) by cost-effective sol-gel approach: analysis of structure, elastic, thermal, and magnetic properties. JOURNAL OF MATERIALS SCIENCE-MATERIALS IN ELECTRONICS **31**(12), 9726–9741 (2020)
49. M.A. Maksoud, G.S. El-Sayyad, H.S. El-Bastawisy, R.M. Fathy, Antibacterial and antibiofilm activities of silver-decorated zinc ferrite nanoparticles synthesized by a gamma irradiation-coupled sol–gel method against some pathogenic bacteria from medical operating room surfaces. RSC Adv. **11**(45), 28361–28374 (2021)
50. A. El-ghandour, A.S. Awed, M.I.A. Abdel Maksoud, M.A. Nasher, 1,2-Dihydroxyanthraquinone: Synthesis, and induced changes in the structural and optical properties of the nanostructured thin films due to γ-irradiation. Spectrochim. Acta Part A Mol. Biomol. Spectrosc. **206**, 466–473 (2019)
51. A.M. Rashad, A.E.I. Helal, G. Ahmed, S. Kassem, R. Fahim, S. Salem, S.E.-D. Mohamed, A. Gamal, Spectroscopic Analysis of Irradiated Natural Quartz and ESR dating aspects. Arab. J. Nucl. Sci. Appl. **53**(3), 197–209 (2020)
52. B. Alshahrani, H.I. ElSaeedy, A.H. Korna, H.A. Yakout, M.I.A. Maksoud, R.A. Fahim, M. Gobara, A.H. Ashour, The effect of Ce3+ doping on structural, optical, ferromagnetic resonance, and magnetic properties of ZnFe2O4 nanoparticles. J Mater Sci: Mater Electron **32**(1), 780–797 (2021)
53. M.I.A.A. Maksoud, S.M. Kassem, M. Bekhit, R.A. Fahim, A.H. Ashour, A.S. Awed, Gamma radiation shielding properties of poly(vinyl butyral)/Bi2O3@BaZrO3 nanocomposites. Mater. Chem. Phys. **268**, 124728 (2021)
54. B. Alshahrani, H.I. ElSaeedy, S. Fares, A.H. Korna, H.A. Yakout, M.I.A.A. Maksoud, R.A. Fahim, A.H. Ashour, A.S. Awed, The effect of gamma irradiation on structural, optical, and dispersion properties of PVA/Zn0.5Co0.4Ag0.2Fe2O4 nanocomposite films. J. Mater. Sci.: Mater. Electron. **32**(10), 13336–13349 (2021)
55. B. Alshahrani, H.I. ElSaeedy, A.H. Korna, H.A. Yakout, A.H. Ashour, M.I.A.A. Maksoud, R.A. Fahim, A.S. Awed, Revealing the effect of gamma irradiation on structural, ferromagnetic resonance, optical, and dispersion properties of PVC/Mn05Zn-05Fe2O4 nanocomposite films. Opt. Mater. **118**, 111216 (2021)
56. A. Madhu, B. Eraiah, N. Srinatha, Gamma irradiation effects on the structural, thermal and optical properties of samarium doped lanthanum–lead- boro-tellurite glasses. J. Lumin. **221**, 117080 (2020)
57. R.K. Brow, The structure of simple phosphate glasses. J. Non-Cryst. Solids **263**, 1–28 (2000)
58. S.W. Martin, Ionic conduction in phosphate glasses. J. Am. Ceram. Soc. **74**(8), 1767–1784 (1991)
59. R.K. Brow, C.A. Click, T.M. Alam, Modifier coordination and phosphate glass networks. J. Non-Cryst. Solids **274**(1–3), 9–16 (2000)
60. S. Abo-Naf, M. El-Amiry, A. Abdel-Khalek, FT-IR and UV–Vis optical absorption spectra of γ-irradiated calcium phosphate glasses doped with Cr2O3, V2O5 and Fe2O3. Opt. Mater. **30**(6), 900–909 (2008)
61. A.M. Efimov, IR fundamental spectra and structure of pyrophosphate glasses along the 2ZnO· P2O5–2Me2O· P2O5 join (Me being Na and Li). J. Non-Cryst. Solids **209**(3), 209–226 (1997)
62. C. Hermansen, J.C. Mauro, Y. Yue, A model for phosphate glass topology considering the modifying ion sub-network. J. Chem. Phys. **140**(15), 154501 (2014)
63. N. Elalaily, A. Zahran, E. Saad, O. Sallam, F. Ezz-Eldin, Corrosion and infrared study of some γ-irradiated lead-phosphate glasses doped with MoO3. SILICON **10**(4), 1613–1623 (2018)
64. V. Rai, B.R. Sekhar, P. Tiwari, R. Kshirsagar, S. Deb, Spectroscopic studies of gamma irradiated Nd doped phosphate glasses. J. Non-Cryst. Solids **357**(22–23), 3757–3764 (2011)
65. Y.B. Saddeek, M. Kaid, M. Ebeid, FTIR and physical features of Al2O3–La2O3–P2O5–PbO glasses. J. Non-Cryst. Solids **387**, 30–35 (2014)
66. F.H. ElBatal, M.A. Ouis, R.M. Morsi, S.Y. Marzouk, Interaction of gamma rays with some sodium phosphate glasses containing cobalt. J. Non-Cryst. Solids **356**(1), 46–55 (2010)
67. N. Elalaily, A. Zahran, O. Sallam, F. Ezz Eldin, Structure and electrical conductivity of ɤ-irradiated lead–phosphate glass containing MoO3. Appl. Phys. A **125**(2), 1–12 (2019)
68. L.W. Hobbs, F.W. Clinard Jr., S.J. Zinkle, R.C. Ewing, Radiation effects in ceramics. J. Nucl. Mater. **216**, 291–321 (1994)
69. M. Archidi, M. Haddad, A. Nadiri, F. Benyaïch, R. Berger, Defect centers in X-irradiated alkali phosphate glasses: EPR studies. Nucl. Instrum. Methods Phys. Res., Sect. B **116**(1–4), 145–149 (1996)
70. G. Sharma, K. Singh, S. Mohan, H. Singh, S. Bindra, Effects of gamma irradiation on optical and structural properties of PbO–Bi2O3–B2O3 glasses. Radiat. Phys. Chem. **75**(9), 959–966 (2006)
71. F. Piao, W.G. Oldham, E.E. Haller, Ultraviolet-induced densification of fused silica. J. Appl. Phys. **87**(7), 3287–3293 (2000)
72. F. Piao, W.G. Oldham, E.E. Haller, The mechanism of radiation-induced compaction in vitreous silica. J. Non-Cryst. Solids **276**(1–3), 61–71 (2000)
73. V. Dimitrov, Y. Dimitriev, Structure of glasses in PbO-V2O5 system. J. Non-Cryst. Solids **122**(2), 133–138 (1990)
74. H.K. Dan, N.D. Trung, T. Le, N. Le Thai, N.M. Ty, D. Zhou, J. Qiu, Influence of F− on the reduction process of Eu3+ to Eu2+ and optical properties of Eu3+/Eu2+–Er3+–Yb3+ co-doped niobate silicate glasses. J. Non-Cryst. Solids **581**, 121417 (2022)
75. H.K. Dan, D.-N. Le, H.T. Nguyen-Truong, T.D. Tap, H.X. Vinh, N.M. Ty, R. Wang, D. Zhou, J. Qiu, Effects of Y3+on the enhancement NIR emission of Bi+-Er3+ co-doped in transparent silicate glass-ceramics for Erbium-doped fiber amplifier (EDFA). J. Lumin. **219**, 116942 (2020)
76. H.K. Dan, N.M. Ty, T.D. Tap, D.-N. Le, L.T. Vinh, D. Zhou, J. Qiu, Energy transfer and spectroscopic properties of Cr3+/Yb3+ co-doped TeO2–ZnO–La2O3 tellurite glasses under different wavelength excitation lights. Opt. Mater. **100**, 109662 (2020)
77. G. Venkataiah, P. Babu, I.R. Martín, K. Venkata Krishnaiah, K. Suresh, V. Lavín, C.K. Jayasankar, Spectroscopic studies on Yb3+-doped tungsten-tellurite glasses for laser applications. J. Non-Cryst. Solids **479**, 9–15 (2018)
78. H. Zeyada, M. El-Nahass, I. Elashmawi, A. Habashi, Annealing temperatures induced optical constant variations of methyl violet 2B thin films manufactured by the spin coating technique. J. Non-Cryst. Solids **358**(3), 625–636 (2012)
79. D. Sell, H. Casey Jr., K. Wecht, Concentration dependence of the refractive index for n-and p-type GaAs between 12 and 18 eV. J. Appl Phys **45**(6), 2650–2657 (1974)
80. N. El-Ghamaz, A. El-Sonbati, M. El-Mogazy, Effect of γ-radiation on the structural and optical properties of poly (3-allyl-5-[(4-nitrophenyl) diazenyl]-2-thioxothiazolidine-4-one) thin films. J. Mol. Liq. **248**, 556–563 (2017)
81. F. Urbach, The long-wavelength edge of photographic sensitivity and of the electronic absorption of solids. Phys. Rev. **92**(5), 1324 (1953)
82. J. Krumhansl, The Solid State. Annu. Rev. Phys. Chem. **8**(1), 77–104 (1957)
83. S. Wemple, M. DiDomenico Jr., Behavior of the electronic dielectric constant in covalent and ionic materials. Phys. Rev. B **3**(4), 1338 (1971)
84. Y. Caglar, S. Ilican, M. Caglar, Single-oscillator model and determination of optical constants of spray pyrolyzed amorphous SnO 2 thin films. The European Physical Journal B **58**(3), 251–256 (2007)

85. E.D. Palik, Handbook of Optical Constants of Solids (Academic, Orlando, 1985), Google Scholar 286–297
86. H. Ticha, L. Tichy, Semiempirical relation between non-linear susceptibility (refractive index), linear refractive index and optical gap and its application to amorphous chalcogenides. J. Optoelectron. Adv. Mater. **4**(2), 381–386 (2002)
87. D.R. Kanis, M.A. Ratner, T.J. Marks, M.C. Zerner, Nonlinear optical characteristics of novel inorganic chromophores using the Zindo formalism. Chem. Mater. **3**(1), 19–22 (1991)
88. I. Saadeddin, B. Pecquenard, J.-P. Manaud, R. Decourt, C. Labrugère, T. Buffeteau, G. Campet, Synthesis and characterization of single-and co-doped SnO2 thin films for optoelectronic applications. Appl. Surf. Sci. **253**(12), 5240–5249 (2007)
89. C.C. Wang, Empirical relation between the linear and the third-order nonlinear optical susceptibilities. Phys. Rev. B **2**(6), 2045 (1970)